Preparation and Characterization of SiC Thin Films for ^3H_2O Steam Sensing

N. Ait Kaci[a,c,*], S. Kaci[c], K.H. Bentoumi[a], M. Belaid[a], R. Abdelouahab[a], A. Nechaf[a] and A. Lachemet[b]

[a] *Nuclear Research Center of Algiers (CRNA), Frantz Fanon Bd, 2 PB 399 RP, 16000, Algiers, Algeria*
[b] *University of Science and Technology Houari Boumedian (USTHB), Bab Ezzouar, P.B. 32, 16079, Algiers, Algeria*
[c] *Research Center on Semiconductor Technology for Energetic (CRTSE), Frantz Fanon Bd, 2 PB 140 7M, 16038, Algiers, Algeria*

Received: 20.11.2023 & Accepted: 04.03.2024

Doi: 10.12693/APhysPolA.145.336 *e-mail: n.aitkaci@crna.dz

The objective of this study is to elaborate SiC thin film as a humidity sensing element and study its behavior towards tritiated water vapor, to apply it for radiation protection purposes. Silicon carbide was chosen as a material because of its remarkable properties and its capacity to be applied in harsh environments. The thin layers of SiC were deposited on the Si substrate by the magnetron sputtering technique. Their morphological, structural, and optical properties were examined by scanning electron microscopy, X-ray diffraction, and UV visible spectroscopy, respectively. The obtained thin films were examined by X-ray fluorescence and Auger electron spectrometry to get the elemental and chemical state information. The film's sensitivity was carried out by current–voltage measurements of SiC/pSi(100)/Cu Schottky diode structure before and after exposure to tritiated water steam for 10 and 38 days in an airtight container. The impedance measurements were performed in air, at room temperature, with frequencies ranging from 10^{-5} Hz to 0.1 Hz. The current showed an increase in forward bias after exposure to the super-heavy water vapor, which implies that the obtained amorphous SiC thin films could have an application as a tritiated water vapor sensing element at room temperature.

topics: SiC, thin films, ^3H_2O, sensitivity

1. Introduction

In many disciplines, there is still a lot of interest in measuring and tracking the amount of water present in the surrounding air. In particular, sectors including semiconductors, biomedicine, textiles, food processing, pharmaceuticals, meteorology, microelectronics, agriculture, structural health monitoring, and environmental monitoring and protection employ humidity sensors extensively for this purpose. For humidity sensing, materials such as carbon nanotubes (CNTs) and metal oxides are being investigated [1]. Researchers have recently investigated two-dimensional (2D) materials, such as graphene, for applications in humidity sensing [2]. When choosing a humidity sensing component, several criteria must be taken into account, including long-term stability, test reproducibility, cost of fabrication, and shape control.

However, when used in harsh environments, humidity sensors based on metal oxides and CNTs may face several difficulties, particularly those that rely on nuclear-based technologies that must contend with the emergence of radioactive steam sources.

Tritium is one of the radioactive hydrogen isotopes produced most frequently in nuclear reactors that use heavy water (deuterium oxide, ^2H_2O) as their coolant and neutron moderator. The neutron reactions during nuclear power plant operation cause heavy water (^2H_2O) to change into superheavy water (^3H_2O). In light-water nuclear reactors, the activation of boron in control rods and coolant are additional sources of tritium. Tritium is extremely mobile in groundwater and surface water systems and normally occurs in surface waters at a concentration of 0.4–1.2 Bq/L (10–30 pCi/L) [3]. It can be introduced by food, water, air, or through the skin, however, even in hot, humid weather, the

uptake through the latter route is approximately only half that of inhalation. Due to the tritium effects on human health, numerous regulations have been put in place globally to restrict radioactive emissions below a safe limit of 100 Bq/L for drinking water [4], and the annual limit on intake (ALI) for workers is 1×10^9 Bq in Publication 60 of the International Commission on Radiological Protection (ICRP) [5]. The skin contamination caused by some radioisotopes, such as tritium, cannot be reliably detected by the portable or automatic radiological control systems that are currently available. Consequently, individual checks are not a reliable method of identifying this kind of contamination. The most recent International Atomic Energy Agency (IAEA) recommendations state that contamination and air quality monitoring procedures should be reinforced in situations where personal exposure due to this type of contamination is conceivable [6]. The tritium- and other radioactive isotopes-containing water used in nuclear power reactors is typically fitted with specialized sensors. Where there is water, there is humidity, and it is required to use a humidity sensor, particularly for tritiated water, because it contains the radioactive hydrogen isotope tritium, which poses a radiation hazard when inhaled [7, 8]. The other restriction is related to the corrosive impact of ^3H_2O because of its self-radiolysis [9]. In this situation, it would be ideal to utilize a sensing element made of a very durable material.

The level of tritium that is useable and the concentration in places that may be contaminated must subsequently be determined through additional investigation. Real-time tritium level measurement has proven to be difficult. Currently, calorimeters, beta-scintillators, mass spectrometers, and ion chambers are the most sophisticated instruments for measuring tritium levels [10]. A few of the drawbacks of these measuring systems include the size and/or cost of the equipment, the need for experienced operators, and the fact that the majority of these measurement methods do not give real-time measurements. Depending on the testing environment and the tritium concentration, some of the pricey equipment might not be accurate [10, 11].

Silicon carbide is given a lot of consideration for making humidity sensors because of its remarkable chemical, electrical, and optical capabilities [12–14]. Because of its exceptional surface resilience against chemical corrosion, silicon carbide is particularly well suited for steam sensing for environmental monitoring and protection. Numerous studies have been conducted on the fabrication of Schottky diode sensors based on silicon (Si) and silicon carbide (SiC). In some of the earlier papers, Spetz [15], Savage et al. [16], and Hunter et al. [17] used SiC to manufacture Schottky diode-based sensors. These studies were followed by the contributions of several other research teams [18, 19].

Studies on the behavior of tritium on SiC are also available. At temperatures between 298 and 1073 K, the tritium trapping capacity on the surface of SiC was experimentally estimated to be around 10^{10} Bq/m^2 [20]. Additionally, it was found that tritium was trapped on the surface by isotope exchange and adsorption reactions [20].

Silicon carbide thin films are available in a variety of allotropes, including 4-H, 6-H, and others [21, 22]. They can be generated using physical or chemical techniques, including pulsed laser deposition (PLD), magnetron sputtering, reactive sputtering, radio frequency (RF) sputtering, or direct current (DC) sputtering [22, 23]. As for the chemical techniques, numerous can be mentioned, such as chemical vapor deposition (CVD), plasma-assisted chemical vapor deposition (PACVD), low-pressure chemical vapor deposition (LPCVD), atmospheric pressure chemical vapor deposition (APCVD), and light-assisted chemical vapor deposition (LACVD) [24–26]. As part of our study, we proceed to optimize the deposition of SiC thin films via homemade radio frequency (RF) magnetron sputtering.

For measuring humidity, a variety of sensing methods are available, including electrical (resistive, capacitive), thermally conductive, gravimetric, and optical. For instance, optical sensors for humidity sensing are becoming more popular due to their numerous benefits, including their small size, lightweight, low cost, ability to monitor humidity in real-time in hazardous environments, and remote humidity sensing capability [27–29].

Taking into account what we introduced previously, we were interested in investigating SiC thin layers as a sensitive material to tritiated water steam, motivated by the lack of studies regarding its application in the field since there were no previous reports. In this work, we have studied the sensitivity and affinity properties of SiC thin films to tritiated water vapor. The aim is to develop a sensor system for tritiated water vapor in enclosures contaminated with tritiated water vapor for radiation protection purposes.

2. Experimental part

2.1. Elaboration of SiC thin films

Magnetron sputtering (RF 13.56 MHz) homemade equipment was used to elaborate amorphous silicon carbide thin films onto monocrystalline boredoped silicon (p-Si (100), with resistivity between 1 and 10 Ω cm) and glass substrates. Before cleaning with acetone and ethanol in an ultrasonic bath for 15 min at room temperature, samples of silicon and glass substrates were diced into 10×10 mm^2 chips and rinsed with deionized water. After that, silicon substrates were washed with

TABLE I

Sputtering parameters.

Parameter	Value	
RF power [W]	120	
Ar rate [SCCM]	10	
source-target distance [cm]	10	8
sputteing time [min]	60	180
SiC thickness estmation [nm]	190	1189
pressure [mBar]	10^{-2}	

40% hydrofluoric acid (HF) to remove the native oxide from the surface and then rinsed with deionized water before being placed in the deposition chamber. All samples were dried with a stream of dry nitrogen. A turbo-molecular pump was then used to pump the closed chamber up to about 10^{-6} mbar (10^{-4} Pa).

In the beginning, the chamber was pressurized with 40 SCCM of pure argon (N60) for 10 min to provide an environment completely free of contaminants for the deposition process. After that, pumping was continued until the vacuum resumed at about 10^{-6} mbar. The SiC target was pre-sputtered for 10 min before deposition to clear any potential surface imperfections.

We have investigated the variation of some sputtering parameters influencing the development of thin layers for SiC thin layer deposition, as shown in Table I. We kept the argon flow at 10 SCCM, and the overall pressure in the chamber was 10^{-2} mbar. The distance between the 6H–SiC target and substrate holder was tuned as shown.

The magnetron cathode receives a voltage, which imposes a set working power of 120 W. For this study, two sputtering times, 60 and 180 min, were used, and the deposition was made at room temperature.

The optimization of the sputtering deposition parameters aims to choose the protocol giving the greatest deposition thickness, and in our case, the thickness was around 1 μm. Indeed, the parameters of the deposition protocol are: deposition time of 180 min, pressure of 10^{-2} mBar, power of 120 W, Ar flow rates of 10 SCCM, and sample source distance of 8 cm. The apparatus used in this work is shown in Fig. 1.

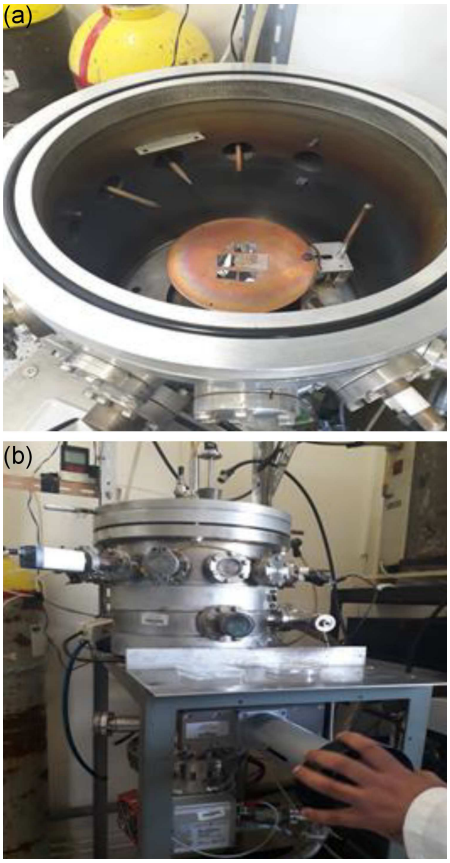

Fig. 1. (a) Top view and (b) overall view of magnetron sputtering equipment.

2.2. Characterizations

The SiC thin layers were elaborated by the magnetron sputtering technique, and their morphology was examined by JSM-7610FPlus high-resolution scanning electron microscope (SEM). The work distance (WD) was 2.8 mm, the accelerating voltage was 11.4 kV with an electron secondary beam, and the vacuum level was 10^{-4} Pa, without prior sputtering.

Optical characterization was done by UV-Vis spectrophotometry. The Varian Cary 500 ultraviolet–visible–near infrared (UV–Vis–NIR) spectrometer was used, which allows us to evaluate a large set of properties of thin layers, such as the optical gap (E_g), by measuring the absorption, transmission, and/or diffuse reflectance in the range of wavelengths between 250 and 2500 nm.

The X-ray fluorescence (XRF) analysis was carried out with an Amptek EXP-1 XRF spectrometer kit to determine the surface composition and the presence of impurities. The data were taken at room temperature, and the scans were done with a PW2440 goniometer with a flow detector, at a voltage and current of 32 kV and 125 mA, respectively.

Auger electron spectroscopy (AES) analysis was done by Perkin Elmer scanning Auger microprobe, model PHI 660, with an intensity of 1 μA. The electron acceleration voltage was fixed at 3 kV. The argon gun (Ar^+, 4 keV) placed at 15° to the sample surface and an argon beam forming an angle of 75° with the sample normal (located in the analysis chamber) are used to strip the sample during the analysis. The objective of this analysis is to characterize the atoms present on the sample surface, identify the nature of their bindings, and give an idea about thin layer thicknesses.

Crystallography characterization of SiC thin layer deposited on Si substrate was examined by X-ray diffraction (XRD) measurements, for normal incidence, performed on an X'Pert PRO (Philips) diffractometer using monochromatic copper radiation (Cu K_α, $\lambda = 0.1541$ nm) at 40 kV and 40 mA over the 2θ range (5–90°), and for grazing incidence, performed on an X'Pert PRO (Philips) diffractometer using monochromatic copper radiation (Cu K_α, $\lambda = 0.1541$ nm) at 30 kV and 40 mA, with a grazing angle of $\Omega = 0.350°$, over the 2θ range 25–67°.

The measurement of the surface resistivity of thin films was done using the four-point setup.

Current–voltage characterization was performed with an Autolab potentiostat station. The current–voltage characteristic (I–V) defines how much current passes through the diode and what voltage can be measured across the diode. We have studied this characteristic to determine the type of the diodes. The final sensors were exposed to tritiated water, and I–V characterization was done.

To collect the profile of the current–voltage curve, we made electrical connections by connecting the working electrode to the sensor's rear contact and the counter electrode to the sensor's front contact, which is located on the thin layer of SiC. The current–voltage (I–V) parameters chosen are presented in Table II.

The impedance measurements at frequencies from 10^{-5} to 0.1 Hz were measured at open-circuit potential with an alternating current (AC) perturbation voltage of 10 mV at room temperature.

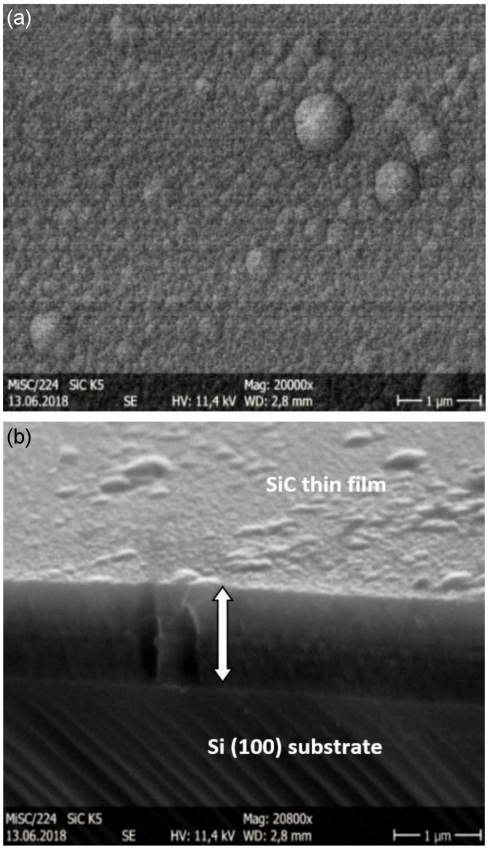

Fig. 2. SEM pictures of SiC thin film — (a) plan view and (b) cross-sectional view — obtained by radio frequency magnetron sputtering technique.

3. Results and discussion

3.1. Morphological characterization

Plan and cross-sectional views of SEM pictures, presented in Fig. 2, clearly show a well-deposited thin film with a good distribution of the particles over the entire observed surface, which indicates a homogeneous deposit. The estimation of the thickness revealed an average of approximately 1 μm, as shown in Fig. 2b.

3.2. Optical characterization (transmittance measurement, band gap determination, and thickness estimation)

From the transmittance spectrum obtained, we can see the presence of interference fringes due to multiple reflections inside the analyzed layer, as shown in Fig. 3a. We can extract thickness of the layer, refractive index, absorption coefficient, etc. These are calculated by the TSTO software based on the Visual Basic programming language.

TABLE II

Current–voltage (I–V) characterization parameters.

Parameter	Value
voltage end [V]	+2
voltage step [V]	0.0244
rate [V/s]	0.01
voltage begins [V]	−2

The band gap energies (E_g) of SiC are calculated by the intersection of the linear portion of the curve $(\alpha h\nu)^n = f(h\nu)$ with energy axis, with $n = 2$ for direct gap materials and $n = 1/2$ for indirect gap materials [30], as represented in Fig. 3b.

In this case, the SiC layer elaborated by sputtering has $E_g = 1.8$ eV and a thickness of 1.1189 μm.

3.3. X-ray fluorescence (XRF) analysis

Figure 4 shows the XRF analysis of a SiC thin film sample. The quantification results of all the elements are given in Table III.

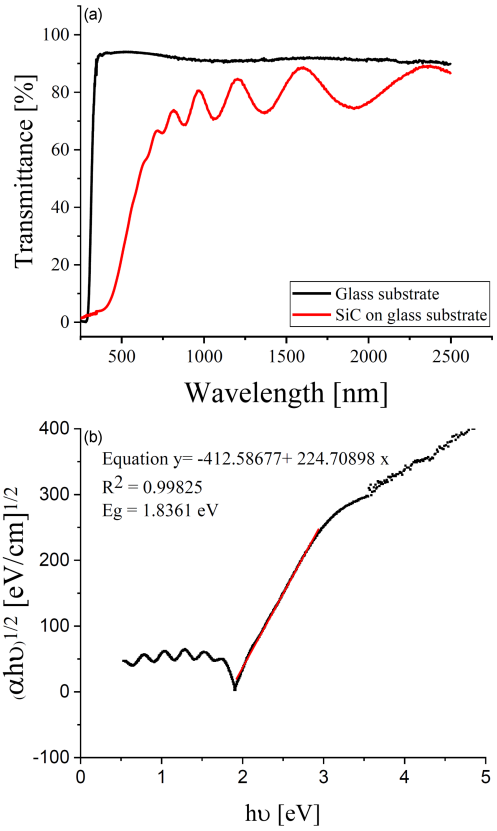

Fig. 3. (a) Optical transmittance spectra and (b) band gap energy.

TABLE III

Quantification results of a SiC thin film sample by X-ray fluorescence.

Analyte	Concentration [%]
Si	88.712
O	6.369
C	4.919

The results show the predominant presence of Si, with 88.71% belonging to both substrate and thin film. In addition, we noted the presence of C at 4.92% and O at 6.37%, the latter of which resulted from the native oxidation of the Si substrate.

3.4. Auger electron spectroscopy (AES) analysis

The Auger electron spectrum of the SiC thin film deposited on a Si substrate for various sputtering times is shown in Fig. 5. It can be seen that the peaks that correspond to the different Auger transitions are well separated. The presence of carbon (C KLL), silicon (Si LMM), and oxygen (O KLL) at the surface is observed, which is in concordance with the previous XRF results. The oxygen peak (515 eV) is due to the native oxide [31].

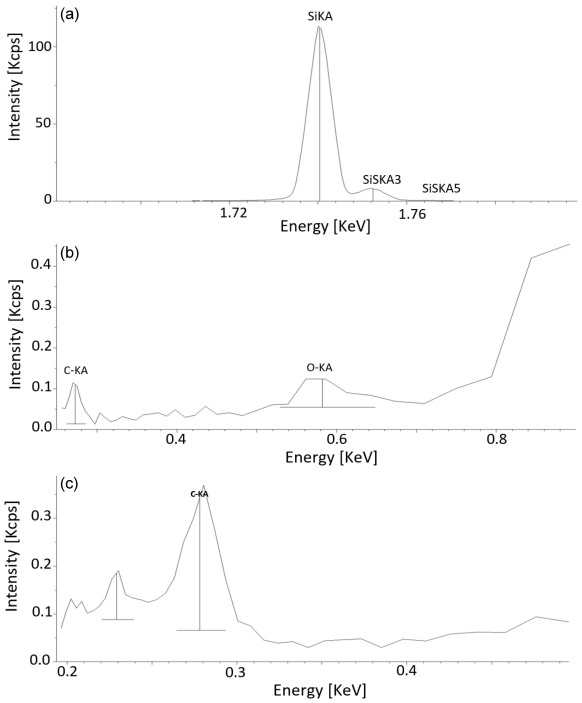

Fig. 4. XRF analysis of the SiC thin film.

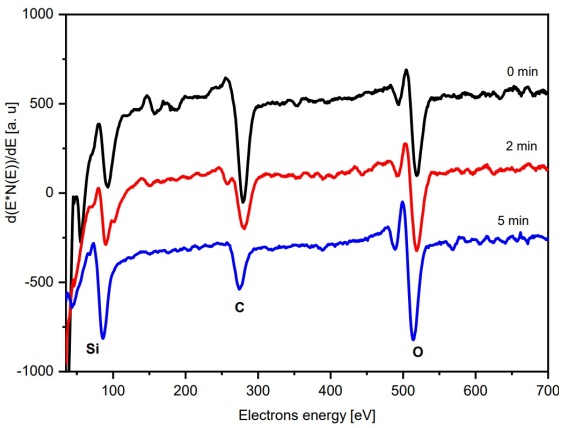

Fig. 5. Auger electron spectra of SiC thin layers deposited on Si substrates for different sputtering times in AES.

There is also a slight shift in the energy of the Si peak (from 94 to 87 eV) as the analysis goes deeper. This is probably because the SiC film, as well as the Si substrate, are semiconductors. Indeed, the energy shift is probably due to the chemical environment, which causes depletions due to the charge phenomenon [32].

It is possible to determine the concentration of the components of the thin layer by measuring the intensity of the lines. The atom concentrations of elements composing the SiC thin layer deposited onto the Si substrate for different sputtering times are shown in Fig. 6. It was noted that the concentration of carbon (C) partially decreases with increasing

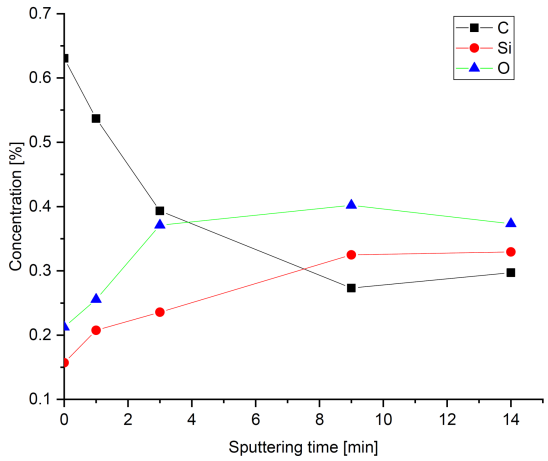

Fig. 6. Atomic concentration of SiC thin layers deposited onto Si substrates for different sputtering times in AES.

sputtering time; on the other hand, the concentrations of silicon (Si) and oxygen (O) increase with increasing sputtering time. This is probably due to the disappearance of the SiC layer until reaching the Si substrate. After 14 min of sputtering, carbon was still found. This is because the SiC thin layer is considerably thick (more than 1 μm), while the (AES) technique is limited to a few nanometers [33].

3.5. X-ray diffraction (XRD) analysis

The X-ray diffraction patterns of Si substrate and SiC/Si were investigated at normal and grazing incidences. For all analyses, the identification was done with HighScore Plus analysis software. Figure 7 shows the normal incidence X-ray diffraction patterns of the Si substrate. The spectrum obtained contains a peak at $2\theta = 69.3°$ of very high intensity, characteristic of the Si (100) substrate, and another peak at $2\theta = 33.08°$ of very low intensity, which is attributed, according to the literature, to the (200) plane of silicon. This is due to the double diffraction of the Si substrate [34].

Figure 8 shows normal incidence X-ray diffraction patterns of unannealed SiC thin layers (in red) and SiC thin layers annealed at 500°C for 2 h (in green).

According to the XRD patterns obtained without thermal treatment, the thin film deposited is completely amorphous, which is in accordance with previous research [34, 35]. For the one obtained after annealing at 500°C for 2 h, another peak is observed at $2\theta = 43.6°$, which shows the beginning of crystallization of the amorphous material attributed to the 4H–SiC phase [34].

To see the impact of annealing on the structural characterization of SiC thin films, these were later subjected to another thermal treatment at 900°C. Figure 9 shows the grazing incidence

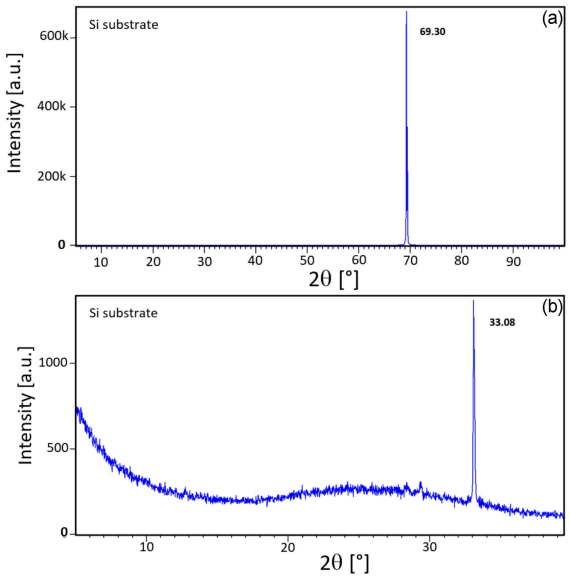

Fig. 7. (a) Normal incidence X-ray diffraction patterns of Si substrate and (b) the normal incidence X-ray diffraction patterns of Si substrate in the 2θ range 5–39°.

TABLE IV

Resistivity values of SiC thin layers on Si substrates.

Sample thickness [m]		V/I ($\times 10^{-4}$) [Ω]	$R_\square$ ($\times 10^{-4}$) [Ω]	ρ ($\times 10^{-11}$) [Ω m]
1.9×10^{-7}	1	0.253	1.15	2.18
	2	0.434	1.97	3.74
12.0×10^{-7}	1	1.27	5.77	69.3
	2	1.06	4.80	57.6
	3	1.33	6.05	72.5
	4	1.45	6.59	79.1

X-ray diffraction patterns of the Si substrate, unannealed SiC thin layer on the Si substrate, and SiC thin layer on the Si substrate annealed at 900°C under Ar gas.

By comparing the obtained results, it was noticed that after the sample was annealed, the peak at $2\theta = 52.02°$ appeared with more intensity. This peak was classified as unknown and has been associated with the SiC polymorph phase in some research, while it is commonly classified as C or Si phases in other studies [36, 37]. This shows that the crystallization of the amorphous material is greater at the surface.

3.6. Resistivity measurement

Table IV summarizes the resistivity values of SiC thin layers deposited on Si substrates with two thicknesses of SiC thin layers. We noted that the resistivity values ranged between 2.18×10^{-11}

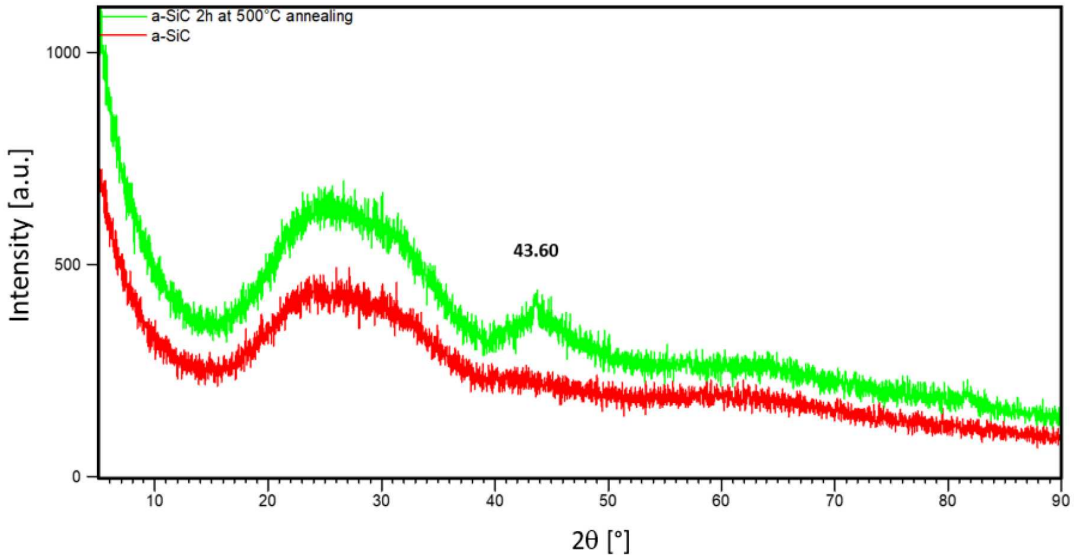

Fig. 8. Normal incidence X-ray diffraction patterns of unannealed SiC thin layers and SiC thin layers annealed at 500°C.

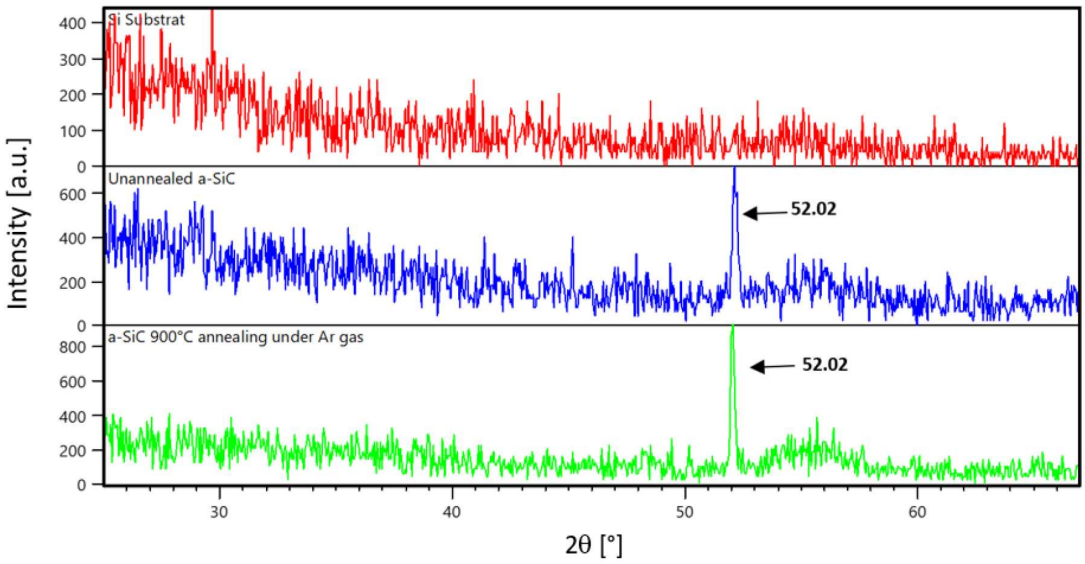

Fig. 9. Grazing incidence X-ray diffraction patterns of Si substrate, unannealed SiC thin layer on Si substrate, and SiC thin layer on Si substrate annealed at 900°C under Ar gas.

and 79.1×10^{-11} Ω m. These values are good since the current could flow fluently, which means that detection will be easy. It should be noted that the electrical resistivity remains greatly influenced by the thickness.

3.7. Current–voltage (I–V) characterization

The exposure of the various sensors to a source of tritium (200 ± 12 Bq) for 10 and 38 days was done, and the results of the response of the three sensors in terms of current with variation of biasing voltage are presented in Figs. 10–12. It can be noted that the responses decrease with low biasing voltage for the sensors except for sensor 1, and after 38 days of exposure, the response increases at relatively high biasing voltage.

At room temperature, we found that the sensors have rectifying properties (Schottky contact) with relatively low reverse current compared to direct current. The direct current of the three sensors decreases at high durations of tritiated water exposure. The sensors observed a significant change in tritiated water in the forward bias. However, there is no significant change in reverse current, as presented in Figs. 10–12.

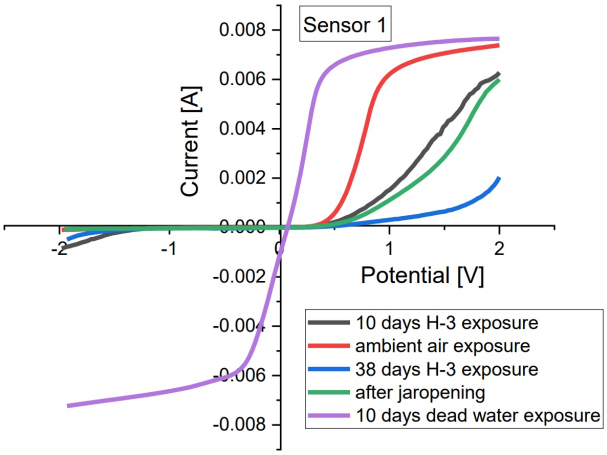

Fig. 10. *I–V* characterization for different tritiated water steam exposures of sensor 1.

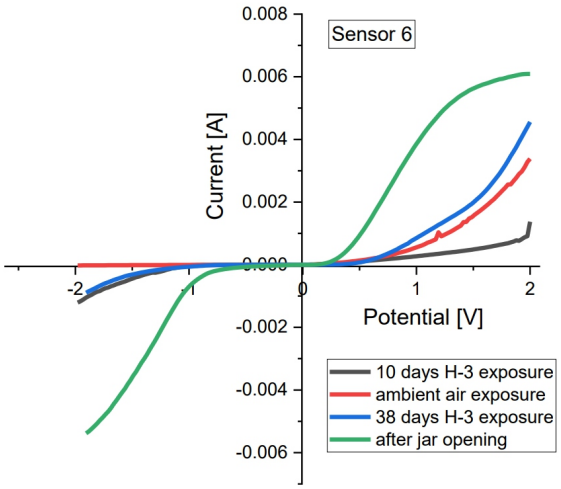

Fig. 11. *I–V* characterization for different tritiated water steam exposures of sensor 6.

After opening the jar, we note that sensor 1 resets, i.e., it returns to its initial position (in ambient air before exposure). Therefore, it is clear that our sensor is sensitive to tritiated water steam, probably due to the adsorption of the steam (Fig. 10).

It was noticed from the current–voltage (*I–V*) characterization that the tritiated water vapor has a reducing behavior. The current–voltage (*I–V*) characteristics, in air and after tritiated water vapor exposure for 10 days, revealed that, at a positive fixed bias potential in the forward bias potentials, the current decreases upon exposure to the reducing vapor. Such a decrease in the current may be induced by the reduction of pre-adsorbed oxygen atoms. The initially adsorbed oxygen molecules on the SiC surface tend to form oxygen ions because of the electron transfer from the SiC surface conduction band to the oxygen atoms [38], leading to further holes in the network. Indeed, by exposing the sensor to a reducing vapor, molecules react with

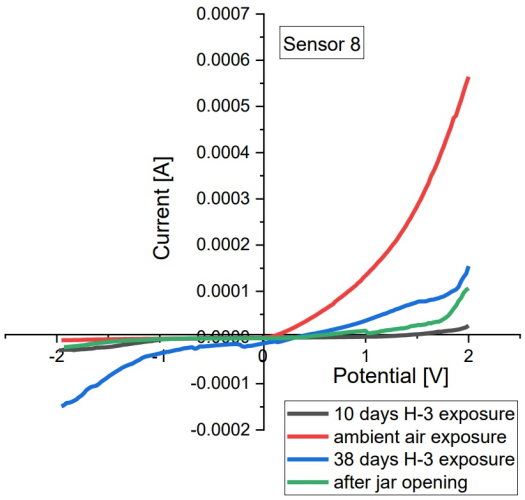

Fig. 12. *I–V* characterization for different tritiated water steam exposures of sensor 8.

pre-adsorbed oxygen atoms on the SiC surface and release electrons to the network, resulting in a decrease in the concentration of the holes in the thin layer and consequently a decrease in the current of the structure [38].

The proposed mechanism was schematized according to the above explanations suggested in order to follow the adsorption–desorption mechanism:

(i) SiC is known to have a hygroscopic nature, meaning it has an affinity for water steam, in our case — tritiated water steam;

(ii) When exposed to humid air, tritiated water molecules from the surrounding environment can be adsorbed onto the surface of the SiC layer;

(iii) The adsorption of water molecules can introduce additional charge carriers (ions) into the SiC material, altering its electrical conductivity;

(iv) As the humidity decreases, the tritiated water molecules may desorb from the SiC surface, causing a corresponding change in the electrical conductivity.

The overall schema is given in Fig. 13.

In order to further see the impact of tritiated water vapor on the behavior of a SiC/Si-based sensor, it is recommended to develop an equivalent circuit diagram. Impedance measurements were performed. Figure 14a displays the Nyquist plot measurement for the sensor in air. A model of the equivalent circuit of SiC/Si heterostructure is proposed to be formed by a series connection of the bulk resistance and the interface impedance, which is constituted of a parallel connection of a resistance and a capacitance at the interface. The electrical equivalent circuit model is derived from the contribution of SiC thin film and the silicon substrate.

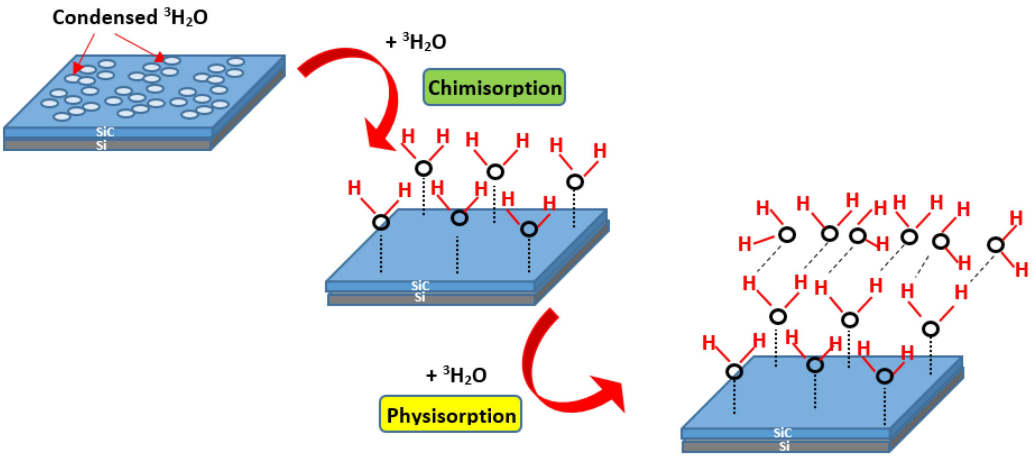

Fig. 13. Schematic representation of the suggested tritiated water vapor sensing mechanism.

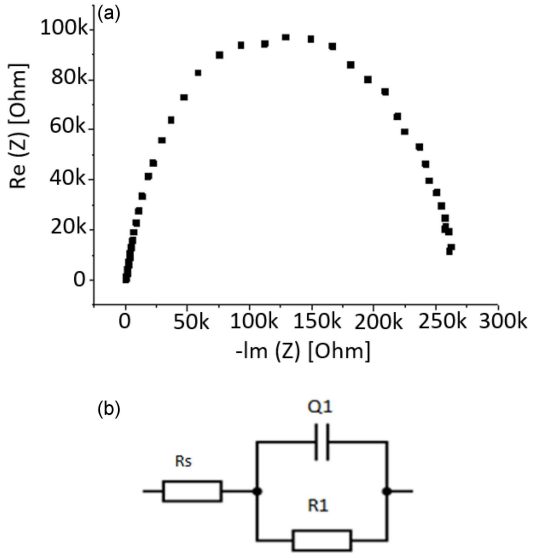

Fig. 14. (a) Nyquist plots of the SiC/Si heterostructure under air as a function of frequency and (b) equivalent circuit diagram of the SiC/Si-based sensor.

A proposed equivalent circuit for the sensor is shown in Fig. 14b. It is composed of the capacitance of the SiC film (Q1) in parallel with the resistance of the SiC film (R1).

3.8. Sensitivity

This formula was used to calculate the sensor's response (S) [39]

$$\frac{\Delta I}{I_{\text{air}}} = \frac{(I_V - I_{\text{air}})}{I_{\text{air}}}, \tag{1}$$

where I_{air} is the sensor's response current when exposed to ambient air, and I_V is the sensor's response current when exposed to tritiated water vapor.

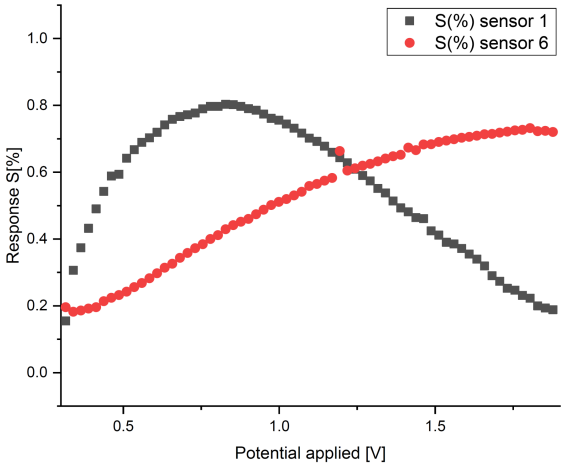

Fig. 15. Response variation to the potential applied for 10 days of exposure.

Figures 15 and 16 show the study of the sensing characteristics in forward bias mode for both time exposures (10 and 38 days, respectively) for tritiated water vapor exposure, with different sensors (sensor 1 and sensor 6). The sensors were biased at voltages in the range where their responses are optimal, as determined in Figs. 15 and 16.

After 10 days of exposure (see Fig. 15), the results show that the response of sensor 1 (marked in black) increases until 0.8 V with a maximum response of 0.8% and then decreases with increasing biasing voltage. For sensor 6 (marked in red), the results show that the response decreases with increasing biasing voltage.

It can be noted that the high response was obtained for low biasing voltages except for sensor 6.

After 38 days of exposure (see Fig. 16), the results show that the response of sensor 1 (marked in black) is lower in comparison with sensor 6 (marked in red), with a maximum response of 0.8, and then decreases with increasing biasing voltage.

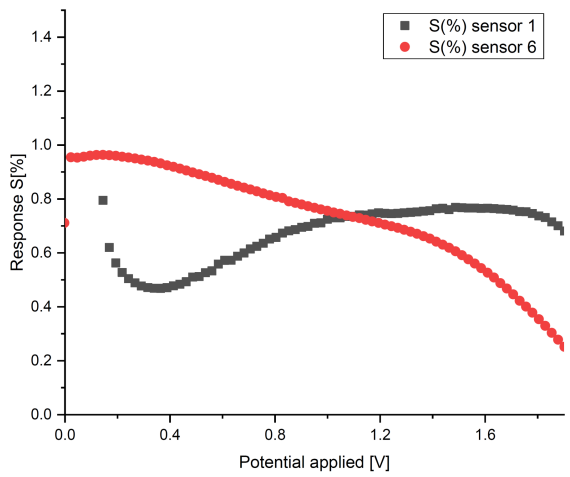

Fig. 16. Response variation to the potential applied for 38 days of exposure.

For sensor 6, the results show that the response decreases with increasing biasing voltage and also that long exposure of the sensor increases the response. It can be noted that the high response was obtained for low biasing voltage; the maximum response was 0.96% for 0.14 V.

The high response at low biasing voltage is an important advantage that allows for low power consumption.

4. Conclusions

This work aims to investigate SiC thin films as a new sensitive material for tritiated water vapor in enclosures potentially contaminated with tritiated water vapor for radiation protection purposes. The obtained results clearly show the feasibility of studying the sensitivity and affinity of SiC to tritiated water vapor following an adsorption–desorption mechanism. A model of a tritiated water vapor sensor was designed based on the fabrication of SiC thin layers of 1 μm thickness and gap energy (E_g) of 1.8 eV on a Si substrate [SiC/pSi(100)/Cu], by the sputtering magnetron technique.

The SEM results indicate that the produced SiC thin film was deposited efficiently and uniformly. The XRD results revealed that the SiC thin films are completely amorphous, with a major presence of Si of 88.7%, C of 4.9%, and O of 6.4% due to the native oxidation of the SiC thin film, observed by XRF analysis.

The impedance measurements, performed in air, and the fitting of the Nyquist plots revealed that the SiC/Si-based sensor heterostructure was formed by a series connection of the bulk resistance and the interface impedance, which is constituted of a parallel connection of resistance and a capacitance at the interface.

The current–voltage (I–V) profile results show that the metal-semiconductor contact is of the Schottky type. According to the obtained results, a considerable shift in sensor responses to tritiated water steam exposure proves the sensor's sensitivity to tritiated water steam, which clearly suggested that the obtained amorphous SiC thin films could have a potential application as a sensing element in a ^3H_2O sensor at room temperature.

Acknowledgments

This work was completed thanks to the Algerian Funds of CRNA/COMENA/MEM and the National Funds of Research CRTSE/DGRSDT/MESRS.

References

[1] A.K. Burcu, *ACS Appl. Electron. Mater.* **4**, 4797 (2022).

[2] B. Shivananju, H.Y. Hoh, W. Yu, Q. Bao, *Electon. Opt. Mater.* **1**, 379 (2019).

[3] M. Ojovan, W. Lee S. Kalmykov, *An Introduction to Nuclear Waste*, 3rd ed., Elsevier, 2019, p. 145.

[4] People's Democratic Republic of Algeria, Executive Decree No. 11-125, 2011.

[5] H. Smith, 1990 International Commission on Radiological Protection, Annals of the ICRP Vol. 21, Oxfordshire, Didcot 1990.

[6] IAEA Safety Standards, *Occupational Radiation Protection, General Safety Guide*, GSG-7, IAEA Publishing Section, Vienna 2018.

[7] Z. Franić, *Arh. Hig. Rada Toksikol.* **47**, 359 (1996).

[8] National Library of Medicine, PubChem Compound Summary for Tritium, 2023.

[9] S. Sanguanmith, J. Meesungnoen, C.R. Stuart, P. Causey, J.-P. Jay-Gerin, *RSC Adv.* **8**, 2449 (2018).

[10] J.A. Parker, M.D. Aspinall, C. Boxall, F.D. Cave, M.J. Joyce, *Prog. Nucl. Energy* **162**, 104733 (2023).

[11] J.R. DeVore, M.A. Buckner, *Tritium Monitoring Techniques* 1996.

[12] E.J. Connolly, H.T. Phum, J. Groeneweg, P.M. Surro, P.J. French, in: *17th IEEE Int. Conf. Micro Electro Mechanical Systems (MEMS 2004), Maastricht*, IEEE, 2004, p. 193.

[13] N. Wright, A. Horsfall, *J. Phys. D Appl. Phys.* **40**, 6345 (2007).

[14] J. Prakash, R. Venugopalan, B.M. Tripathi, S.K. Ghosh, J.K. Chakravartty, A.K. Tyagi, *Prog. Solid State Chem.* **43**, 98 (2015).

[15] A. Spetz, A. Arbab, I. Lundström, *Sens. Actuators B: Chem.* **15**, 19 (1993).

[16] S. Savage, H. Svenningstorp, L. Unéus, A. Kroutchinine, P. Tobias, L.G. Ekedahl, I. Lundström, C. Harris, A. Lloyd Spetz, *Mater. Sci. Forum* **353**, 747 (2001).

[17] G. Hunter, P. Neudeck, L.Y. Chen, D. Knight, C.C. Liu, Q.H. Wu, *Mater. Sci. Forum* **264**, 1093 (1997).

[18] W.M. Tang, J.P. Puxiang Lai, J.P. Xu, C.L. Chan, *Sensors and Actuators A-physical* **119**, 63 (2005).

[19] L. Sun, B. Wang, Y. Wang, *Adv. Mater. Interfaces* **5**, 1701300 (2018).

[20] A. Arbab, A. Spetz, I. Lundström, *Sens. Actuators B Chem.* **19**, 562 (1994).

[21] K. Katayama, M. Nishikawa, T. Takeishi, in: *Proc. of the 19th IEEE/IPSS Symposium on Fusion Engineering (19th SOFE)*, IEEE, 2002, p. 164.

[22] G.L. Harris, *Properties of Silicon Carbide*, Inspec (1995), p. 282.

[23] X. Kerbiriou, Ph.D. Thesis, University of Orléans, 2006.

[24] P. Krulevitch, A.P. Lee, P.B. Ramsey, J.C. Trevino, J. Hamilton, M.A. Northrup, *J. Microelectomech. Syst.* **5**, 270 (1996).

[25] A. Ellison, J. Zhang, J. Peterson, A.W. Henry, Q. Wahab, J.P. Bergman, E. Janzén, Y.N. Makarov, A. Vorob'ev, A. Vehanen, *Mater. Sci. Eng. B* **61**, 113 (1999).

[26] C.W. Locke, A. Severino, F. La Via, M. Reyes, J. Register, S.E. Saddow, in: *Silicon Carbide Biotechnology: A Biocompatible Semiconductor for Advanced Biomedical Devices and Applications*, Ed. S.E. Saddow, Elsevier, Oxford 2012, p. 17.

[27] A. Oliveros, A. Guiseppi-Elie, S.E. Saddow, *Biomed. Microdevices* **15**, 353 (2013).

[28] H. Zhang, S. Yu, *Electr. Opt. Mater.* **7**, 549 (2023).

[29] D.J. Fray, J.M. Jafferson, in: *Reference Module in Materials Science and Materials Engineering*, 2016.

[30] L.M. Ferrari, S. Taccola, J. Barsotti, V. Mattoli, F. Greco, in: *Organic Flexible Electronics*, Eds. P. Cosseddu, M. Caironi, Woodhead Publishing, 2021 p. 437.

[31] Y. Laaziz, Ph.D. Thesis Tetouan, Abdelmalek Essaâdi University, 2015.

[32] R. Yousefi, B. Kamaluddina, M. Ghoranneviss, F. Hajakbari, *Appl. Surf. Sci.* **255**, 6985 (2009).

[33] C. Burggraf, B. Carrière, S. Goldsztaub, *J. Appl. Phys.* **11**, 13 (1976).

[34] R. Saleh, L. Munisa, W. Beyer, *Thin Solid Films* **426**, 117 (2003).

[35] J. Lamon, *Compreh. Nucl. Mater.* **2**, 323 (2012).

[36] G. Brauer, W. Anwand, F. Eichhorn et al., *Appl. Surf. Sci.* **252**, 3342 (2006).

[37] N. Galvão, M. Guerino, T. Campos, K. Grigorov, M. Fraga, B. Manzolli Rodrigues, R. Pessoa, J. Camus, M. Djouadi, H. Maciel, *Micromachanics* **10**, 202 (2019).

[38] S.E. Saddow, D. Alquier, J. Wang, F. LaVia, M. Fraga, *SiC based Miniaturized Devices*, 2020.

[39] J. Kanungo, H. Saha, S. Basu, *Sens. Actuators B Chem.* **140**, 65 (2009).